

## Sound emission on bubble coalescence: imaging, acoustic and numerical experiments

R. Manasseh<sup>1</sup>, G. Riboux<sup>2</sup>, A. Bui<sup>1</sup> and F. Risso<sup>2</sup>

<sup>1</sup>Thermal & Fluid Dynamics, CSIRO  
PO Box 56, Highett, Melbourne, VIC 3190 AUSTRALIA

<sup>2</sup>Institut de Mécanique des Fluides de Toulouse  
UMR 5502 CNRS-INP-UPS, Allée Camille Soula, Toulouse 31400, FRANCE

### Abstract

Laboratory and numerical experiments are presented on the emission of sound on bubble coalescence. The aim was to better understand the fluid-dynamical mechanisms leading to sound emission. Bubbles were formed from a needle. Coordinated high-speed video and acoustic measurements demonstrated that the emission of high-amplitude sound coincided with the coalescence of a primary bubble with a smaller secondary. A numerical simulation was performed using a compressible level-set front-capturing code, in which a compressible gas and nearly compressible liquid are modelled by a single set of the Navier-Stokes equations with a generic equation of state for both phases. In the simulations, the spherical primary and secondary bubbles initially at acoustic equilibrium were brought into contact. The numerical calculations predicted the frequency of emitted sound and the bubble coalescence dynamics very well. The results suggest that the equalization of Laplace pressures could be the mechanism leading to sound emission.

### Introduction

The natural frequency emitted by bubbles oscillating volumetrically with small amplitude has been theoretically predicted and experimentally confirmed for nearly a century [36, 28, 38, 20, 25]. For millimetre-sized bubbles, an excellent approximation to the natural frequency  $f_0$  is given by Minnaert's equation [28],

$$f_0 = \frac{1}{2\pi} \sqrt{\frac{3\gamma P_0}{\rho}} \cdot \frac{1}{R_0}, \quad (1)$$

where  $\gamma$  is the ratio of specific heats of gas inside the bubble,  $P_0$  is the absolute liquid pressure,  $\rho$  is the liquid density and  $R_0$  is the equilibrium bubble radius. However, it is more challenging to explain the mechanism with which bubble sound emissions are initiated. Thus, unlike the frequency, the amplitude of bubble sound emissions is difficult to predict. Passive emission of small-amplitude sound by bubbles is common in many practical industrial flows [10, 3, 24] or environmental flows [27, 6, 22]. The difficulty in predicting the amplitude is one problem in the interpretation of the signals from such sources [3, 24], leading to complex signal-processing approaches [1, 22]. Numerical simulations of compressible multiphase flows, while advancing in quality [e.g. 31, 11, 23, 4] and offering many insights [33] require careful comparison with matching laboratory experiments in order to elucidate the actual excitation mechanism.

Longuet-Higgins [19] proposed three general mechanisms by which the energy giving an initial acoustic perturbation could be imparted to the bubble: (i) a difference in instantaneous Laplace pressure at the instant the bubble is formed; (ii) the radial inrush of liquid as the pinch-off occurs; and (iii) an excitation of the volumetric or 'breathing' mode of the bubble by nonlinear interactions of shape modes [17, 18]. It is likely that some of these mechanisms might apply in some situations, but not in others [12].

Bubbles can emit sound when they pinched off from a parent body of gas. In this case, the excitation mechanism may be a variant of (ii): it has been observed [12] that a high-speed liquid jet penetrates the bubble on the breaking of the neck that joins it to its parent body of gas, and may be responsible for compressing the trapped gas [26]. This phenomenon remains too rapid for experimental quantification, although new ultra-high speed cameras may soon permit pinch-off physics to be studied. Longuet-Higgins [20] also proposed that orifice-formed bubbles could make sound by mechanism (iii).

Bubbles can also emit sound when created by the entrapment of air from a free surface. This might occur in contexts such as raindrop impact [e.g. 35, 34], a plunging jet [e.g. 9, 5] or wave-breaking [e.g. 27, 16, 6, 22]. At the instant the surface closes, pinching off the bubble, there must be a sudden transition from a cavity at atmospheric pressure to a closed bubble in which the pressure exceeds atmospheric by the Laplace pressure due to surface tension, plus the hydrostatic pressure that must now be supported. Thus, in this second class of phenomena, mechanism (i) is a possible explanation as well as (ii) and (iii). Pumphrey & Elmore [35] created bubbles from drop impacts in the laboratory. The amplitude predicted by the Laplace-pressure theory was only about 25% of the experimental values, and the trend with bubble size was not predicted. However, statistical confidence is hard to obtain in drop-impact experiments unless particular experimental procedures are adopted [e.g. 15], because there is considerable variation from drop to drop owing to the natural variation in impact conditions.

The present paper reports experiments and numerical simulations in which bubbles emit sound on coalescence. These bubbles are formed by pinch-off from an orifice but create their loudest sounds on coalescence. Unlike earlier acoustic drop impact studies, repeatability is excellent. Depending on the air flow rate, zero, one, or several coalescences might occur. All mechanisms (i), (ii) and (iii) are conceivable in this case.

### Experimental Method

The general experimental set-up is shown in Figure 1. The test section was a glass tank 1,000 mm high with a square cross-section of 150 mm. The tank was filled with filtered tap water at a temperature between 16 and 17°C. Air bubbles of 1.6 mm diameter were injected at 85 mm from the bottom of the tank by a needle with an internal diameter of 0.1 mm and a length of 100 mm. The rate of bubble production was controlled by adjusting the pressure in the tank to which the needle is connected.

A high-speed digital video camera (Photron Ultima APX) was used to film the bubble detachment from the tip of the needle at a frame rate of 20,000 Hz and with an exposure time of 1/87,600 s. The region imaged was 1.113 mm high and 2.226 mm wide with a resolution 128 × 256 pixels. Images of the bubbles were processed to extract their equivalent spherical radius and location as a function of time [7].

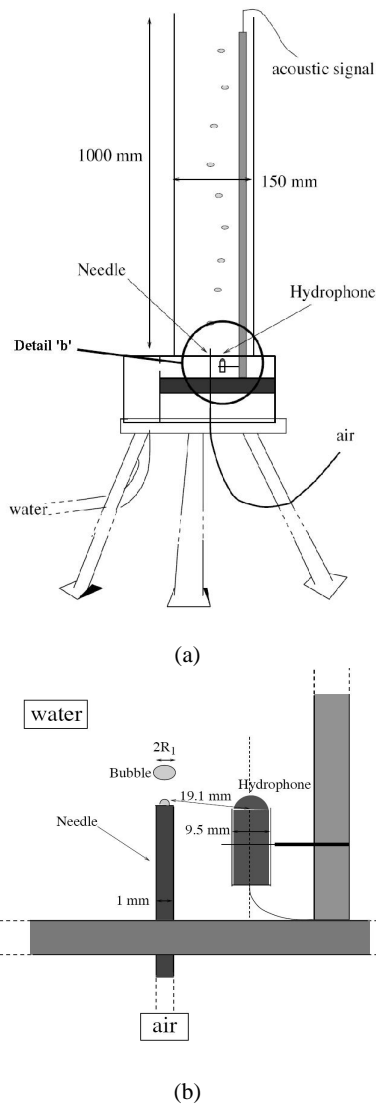


Figure 1: Schematic of the experimental set-up. (a) Tank and air supply. (b) Bubble formation and hydrophone.

A Brüel & Kjaer type 8103 hydrophone was used to transduce the acoustic signal. In the relevant 1-10 kHz band, this hydrophone type has an essentially spherical directivity field, ensuring sounds from any direction are equally transduced, and there is a linear conversion from transduced voltage to pressure based on the hydrophone's individual calibration. The location of the hydrophone relative to the needle was measured with an accuracy of  $\pm 0.1$  mm by taking images in two orthogonal directions. Distances were calculated from the true acoustic centre of the 9.5 mm diameter hydrophone. In the present experiments the distance from the acoustic centre to the bubble centre was  $19.1 \pm 0.1$  mm. The hydrophone's presence caused no disturbance to the bubble formation and rise dynamics.

In a series of initial tests, the hydrophone was traversed in the horizontal and vertical. This was to check that the sound field fell off approximately as  $1/r$ , where  $r$  is the distance from the bubble centre, rather than being significantly affected by sound wave modes or reverberations. Tests were also carried out in larger tanks to confirm that the 150 mm cross-section of the actual tank did not cause any distortion or modification to the acoustic signal created by bubbles formed from the needle. It

is known that as the tank in which bubbles are formed is made smaller, there will eventually be an effect on the acoustic signal [30], although this problem is most marked with tanks of circular rather than square cross-section. For the bubbles created in the present experiments, the tank used was confirmed to be an appropriate size and shape to preclude wall or tank-size effects.

The hydrophone signal was pre-amplified by a Brüel & Kjaer type 2635 charge amplifier set to the individual calibration of the hydrophone. The signal was then fed through a purpose-built high-pass 5-pole Bessel filter with a 500 Hz cut-off and an amplitude gain of 10. The high-pass filtering eliminated any low-frequency pressure fluctuations due to bubble motion while preserving completely the bubble-acoustic signals which were all above 3 kHz. The filtered signal was digitized by a National Instruments Data Acquisition Card type 6024E using high-speed data logging software built on the National Instruments LabView platform. Considering the typical level of background noise, the random error in transduction of the acoustic pressure was less than 10%. This could be improved if necessary with low-pass filtering, but for the present paper this accuracy was sufficient.

The gate signal from the camera was logged on one channel of the datalogging card and the high-pass filtered acoustic signal was logged on a second channel. A nominal logging rate of 120 kHz was used for both channels. However, since a precise comparison of the video and acoustic signals was required, it was noted that no card will in fact digitize data at exactly the requested rate but at a marginally different rate dependent on the card's internal arithmetic; in the present experiments this marginal difference is sufficient to cause a noticeable misalignment of acoustic and video records for the lowest bubble-production rates. The actual logging rate was extracted from low-level routines and was found to be 119,760.48 Hz; its use ensured a comprehensively precise comparison of acoustic and video records.

A digital oscilloscope (Tektronics TDS210) enabled a measurement of the rate of production of primary bubbles, by measuring the interval between pulses. Typically, this could be done with an accuracy of  $\pm 0.1$  s<sup>-1</sup> or less; however, as noted below, for the highest bubble production rates the bubble formation became less regular, giving a bubble-production rate estimation accuracy of  $\pm 0.5$  s<sup>-1</sup>.

The acoustic pressures measured at the hydrophone were converted to the acoustic pressures that would be present at the monitoring point P1 in the numerical simulation (Figure 5), assuming the acoustic field was monopolar. This can be justified by the initial checks that showed the sound pressure amplitude trending approximately as  $1/r$  with distance.

Acoustic time series and photo-montages of the high-speed video frames were generated over the same time window so that acoustic and visual events could be clearly correlated. The original size of the frames, which can be seen in Fig. 3, was 128 pixels wide by 256 pixels high. Given the desired time window and the number of frames available within that time, the width was calculated of a vertical 'strip' of the centre of each frame. For example, to fit 100 frames into a montaged image 400 pixels wide, a vertical strip with the central 4 pixels of each 128 pixel image was inserted into the montaged image at its corresponding time. Since most of the interesting variations occur on the centreline of the bubble image, this technique preserved much of the relevant information content of the high-speed video. In the extreme, a montage of strips each only 1 pixel wide would be a 'time-space diagram' [e.g. 8] showing the rate at which events move along the centreline.

## Numerical methods

The numerical model was based on: i) the level-set method to track the interfaces; and (ii) an explicit flow solver for compressible and nearly incompressible multiphase flows. The gas and liquid are treated as a single continuum fluid with properties varying continuously from gas to liquid states. Coupled with a high-resolution advection scheme, this modelling approach would allow the description of the movement of gas and fluid and the deformation of the interface separating them on a fixed computational mesh [4].

The compressible-nearly incompressible flow solver was based on the solution of an additional differential equation for pressure which was derived from the laws of mass and energy conservation,

$$\frac{\partial p}{\partial t} + \vec{u} \nabla p = -\rho c^2 \nabla \vec{u}, \quad (2)$$

where  $c$  is the sound speed defined as

$$c^2 = \gamma \left( \frac{p + p_\infty}{\rho} \right),$$

where  $p_\infty$  is a stiffness parameter which is zero for the gas.

A generic equation of state of the form

$$\rho e = \frac{p + \gamma p_\infty}{\gamma - 1}, \quad (3)$$

was used, where  $e$  is the internal energy. The parameter  $\gamma$  has the usual meaning of the ratio of specific heats for the gas, but is used in conjunction with  $p_\infty$  to define the compressibility of the liquid.

To track the evolution of the interface, an equation was employed that describes the convection of a level function. This function is chosen as a signed distance function with the zero level set defining the interface location [32], and has the form

$$\phi_t + (\vec{u} \cdot \nabla) \phi = 0. \quad (4)$$

Using the level function, the steep changes of fluid properties across the interface were smoothed out to minimize numerical oscillations in the solution of Navier-Stokes equations. The level function was also used to calculate interfacial geometrical properties, such as the normal vector,  $\vec{n}$ , and the interfacial curvature,  $\kappa$ , as follows:

$$\vec{n} = \frac{\nabla \phi}{|\nabla \phi|}, \quad \kappa = \nabla \cdot \vec{n},$$

which in turn define the surface tension.

The system of differential equations describing the fluid and interface motions was solved using a projection method. This comprised a prediction and a correction steps (see [40]). The high-resolution numerical schemes ENO (Essentially-Non-Oscillatory) or WENO (Weighted ENO) was used for the convective flux calculation.

## Experimental Results

At very low bubble production rates  $f_b$  less than  $3.5 \text{ s}^{-1}$ , a series of single bubbles was formed. High-speed imaging confirmed that there was no coalescence. A very faint signal was detectable on amplification of the hydrophone signal, barely above the background noise, corresponding to the pinch-off of each bubble. In passive-acoustic pinch-off experiments reported earlier [24, 23], the pinch-off process generated sounds audible to the naked ear. The bubbles of the present experiment are

approximately 1.6 mm in diameter, whereas bubbles produced in passive-acoustic pinch-off experiments reported earlier [24] ranged from about 4 to 8 mm in diameter. Hence the present bubbles were one to two orders of magnitude smaller in volume, and thus had much less energy stored on compression and available for acoustic emission.

Once the air flow rate is increased such that the bubbling rate  $f_b$  is above  $3.6 \pm 0.1 \text{ s}^{-1}$ , occasional loud clicks are audible and corresponding sharp spikes appear on an oscilloscope trace. These spikes have an order of magnitude greater amplitude than the sound created on pinch-off. The frequency was  $4.15 \pm 0.5 \text{ kHz}$  which is the Minnaert frequency for a bubble of 1.6 mm diameter. Above an air flow rate of  $3.8 \pm 0.1 \text{ s}^{-1}$ , loud clicks are produced regularly and the spikes are spaced regularly at the bubble production rate. The  $3.8 \pm 0.1 \text{ s}^{-1}$  threshold for this phenomenon was quite repeatable in separate experiments performed over several different days.

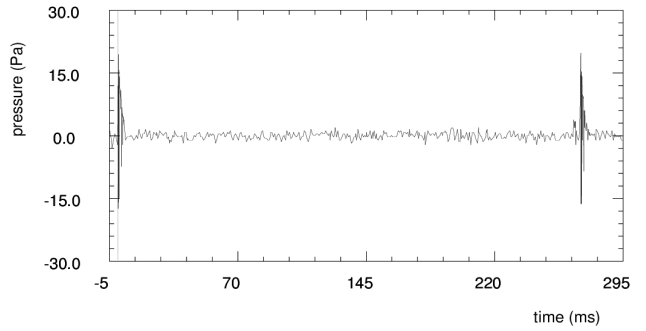


Figure 2: Timeseries of acoustic data over a time of 300 ms, with pressures transformed to values expected at the numerical simulation monitoring point P1 (see Figure 5). Bubble production rate  $3.82 \pm 0.03 \text{ s}^{-1}$ . Series triggered on a pulse at time  $t = 0$ .

The acoustic record over a time window of 300 ms is shown in Fig. 2. Acoustic pressures shown have been transformed assuming a  $1/r$  dependence to the pressures expected at the numerical simulation monitoring point P1. Bubbles were formed from the needle at  $3.8 \text{ s}^{-1}$ , which is about 260 ms apart. The acoustic emissions were a series of sound pulses, an order of magnitude amplitude higher than the background. Each pulse was audible as a single ‘tap’ or ‘knock’ like an individual musical note being struck. These emissions were thus just like any individual bubble-acoustic pulse reported in the literature [e.g. 28, 39, 14, 24]. Close observation of the high-speed video (Fig. 3) shows that a smaller secondary bubble formed immediately after the primary has detached, and soon thereafter coalesced with it. The details of this phenomenon including the size of the bubbles had excellent repeatability. The secondary bubble was much smaller, about a sixth the diameter of the primary. It coalesced with the primary before it had detached itself, thus temporarily re-attaching the primary to the air supply. About 0.1 ms later, it detached itself and was absorbed into the primary. Loud sound emission under circumstances of bubble coalescence has been noted before [13].

The circumstances leading to in-line pairing and subsequent coalescence of orifice-formed bubbles have been studied before, particularly in the chemical engineering literature [29, 2, 37, 21]. However, most detailed coalescence studies are for the pairing and coalescence of equal-sized bubbles.

Thus, each of the “3.8 bubbles per second” is really a primary that has coalesced with a secondary immediately follow-

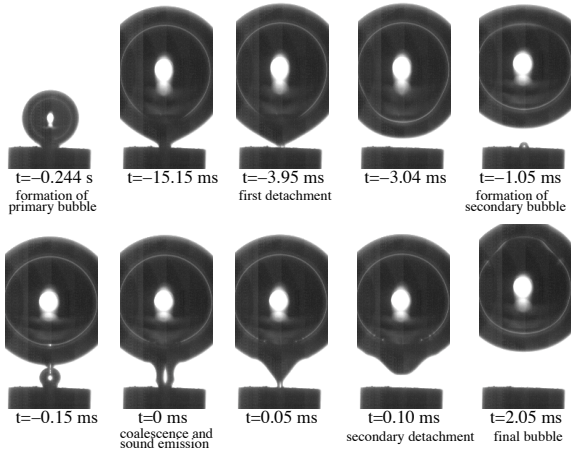


Figure 3: Bubble formation sequence. Bubble production rate  $f_b$  is  $3.8 \text{ s}^{-1}$ , bubble diameter 1.6 mm, as in Figure 2.

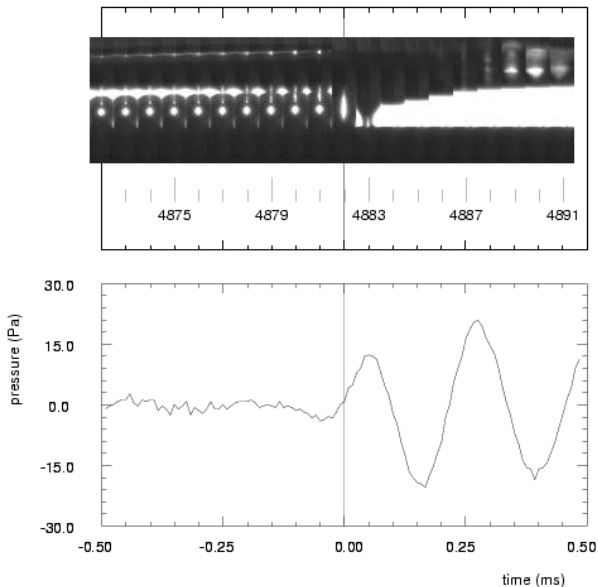


Figure 4: Time-series of video and acoustic data over a time of 1 ms. Bubble production rate  $f_b$  is  $3.8 \text{ s}^{-1}$ , bubble diameter 1.6 mm, as in Figures 2-3. Secondary scale in upper panel shows video frame numbers.

ing, so that over a long time scale they appear to be one bubble. Each formation-and-coalescence event is heard as a single sound pulse. Over the 300 ms timescale, the second formation-and-coalescence event appears as a second pulse about 260 ms later. Furthermore, the sound created on coalescence had an order of magnitude greater amplitude than the sound created on pinch-off.

As the air flow rate is increased, further coalescences occurred with each primary bubble, with the number of coalescences increasing with air flow rate and each coalescence regime being quite repeatable. Like the binary in-line coalescences noted above, multiple coalescences at a needle tip have been observed before with photographic techniques [e.g. 41]. In the present experiment, the production of the primary bubble and all following bubbles that coalesced with it were still clearly separated in time from the production of the next primary bubble. Thus the ‘bubbling rate’  $f_b$  is the rate of production of primary bubbles.

At a bubbling rate of  $25 \pm 0.5 \text{ s}^{-1}$ , up to nine coalescences were observed in the high-speed video data; in this case each of the “25 bubbles per second” is really a bubble formed from the merging of 10 bubbles. Above  $25 \pm 0.5 \text{ s}^{-1}$  bubble production becomes chaotic.

In Fig. 4, the time window shows 1 ms bracketing the coalescence event, for the case of  $f_b = 3.8 \text{ s}^{-1}$  in which only one coalescence per primary occurs. The time  $t = 0$  has been set at the centre time of the frame where coalescence of the primary and secondary bubble occurs. It is clear that the sound pulse is initiated at the very instant of coalescence. It can be noted that prior to sound production, the primary bubble begins to develop a small, downward-pointing ‘nose’ in response to the approach of the secondary bubble. It is clear that sound pressure rises during the coalescence event.

#### Numerical simulations of bubble coalescence

Simulation of bubble coalescence was conducted in an axisymmetric coordinate system. The computational domain size was  $7.68 \times 11.52 \text{ mm}$  (see Figure 5) described by a uniform  $256 \times 384$  computational mesh. The bottom and side walls had no-slip boundary conditions and the top of the domain was free slip. The initial radii of the large and small bubbles were 0.8 mm and 0.125 mm, respectively, to match the experiment. The bubble density and viscosity were set as  $1.2 \text{ kg m}^{-3}$  and  $1.7 \times 10^{-5} \text{ Pa s}$ . The liquid density and viscosity had their physical values of  $1000 \text{ kg m}^{-3}$  and  $0.001 \text{ Pa s}$ . The bubbles were assumed to be filled with an ideal gas with  $\gamma = 1.4$  and  $p_\infty = 0 \text{ Pa}$  and the liquid was assumed to be nearly incompressible with  $\gamma = 7.15$  and  $p_\infty = 3.05 \times 10^8 \text{ Pa}$ . The surface tension coefficient was that of the air-water interface, i.e.  $0.074 \text{ kg s}^{-2}$ . Other parameters and conditions were chosen to match the conditions of the experiment shown in Figures 2- 4. The locations of the initial bubbles and monitoring points are shown in Figure 5.

The predicted shapes of the bubbles at different times before and after the coalescence are shown in Figure 6. In Figure 7, the experimental observations are shown for the same times. It can be seen that there is a very good agreement in the interfacial dynamics of the coalescence event. In the experiment, the secondary was still attached to the air supply on coalescence, hence re-attaching the primary temporarily. The only significant qualitative differences might be attributed to the fact that in the simulation there was no air supply feeding the secondary bubble immediately after a coalescence.

The numerically simulated frequency of pressure oscillation was 4000 Hz, which agrees well with the natural oscillation frequency of the larger bubble predicted by (1), which is ap-

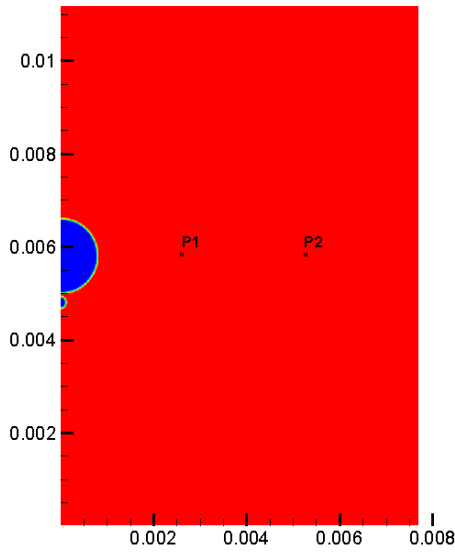


Figure 5: Computational domain with initial bubbles and monitoring points P1 and P2.

proximately 4077 Hz. Furthermore, the numerically simulated frequency is within about 5% of the experimentally measured frequency of about 4150 Hz. The peak pressure at point P1 is about 13 Pa, whereas the experimental data, transformed to point P1, corresponds to about 20 Pa.

### Conclusions

A system in which bubbles coalesced on formation generated loud bubble-acoustic emissions at the instant of coalescence of secondary bubbles with the primary bubble. A compressible-flow numerical model based on the level-set method was able to

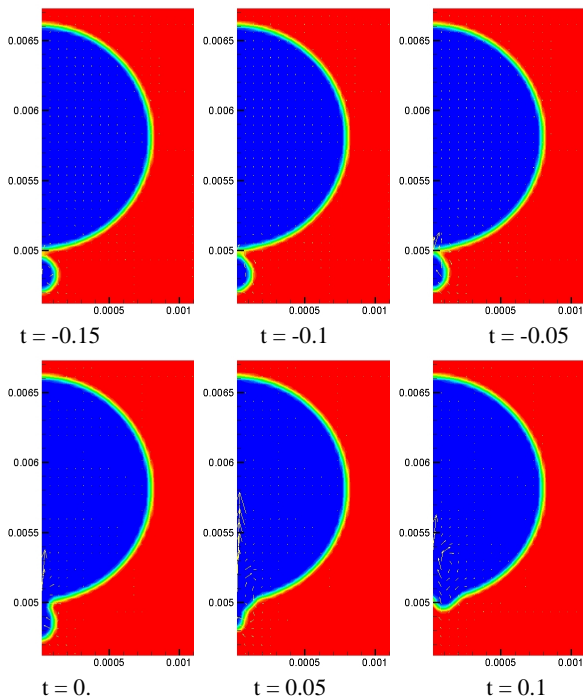


Figure 6: Numerical simulation of the bubble coalescence. Unit for the relative time is ms.

accurately predict both the kinematics of the bubble coalescence event and the frequency of the sound emission. The simulation correctly predicted the sound pressure amplitude rising at the instant of coalescence. The numerical model also obtained an estimate of the sound amplitude in the same order as the experiment.

The numerical domain was over an order of magnitude smaller than the experimental domain and so one would not expect the time series of pressure oscillations to be the same. Nonetheless, the acoustic oscillation frequency of the bubble was predicted to within 5%. The amplitude was less well predicted, being a factor of 1.5-2.0 lower than what would be expected from the experimental data.

The amplitude of the emitted sound was up to an order of magnitude greater than the sound created on pinch-off of the primary bubble. The sound frequency was at the Minnaert frequency of the large bubble. As the air flow rate increased, the size and number of secondary bubbles increased, and the sound amplitude also increased. On coalescence, the sound pressure was found to always rise initially.

The experiments and the numerical simulations agreed that in the present coalescence phenomenon there was no jet penetrating the bubble, as found in experiments on sound generation on pinch-off [12, 26]. Hence, mechanism (ii) seems unlikely. The experiments and the numerical simulations also agreed that sound was emitted at the very instant of bubble coalescence. At the time of sound emission, shape-mode distortions have not yet begun to relax, a process that might generate sound emissions by mechanism (iii). Mechanism (i), the Laplace-pressure equalization phenomenon, appears to have survived this rough elimination. However, more detailed numerical experiments and matching laboratory work would have to be performed to test the Laplace-pressure hypothesis.

Future numerical experiments should attempt to examine the Laplace pressure mechanism (i) versus the shape-mode mech-

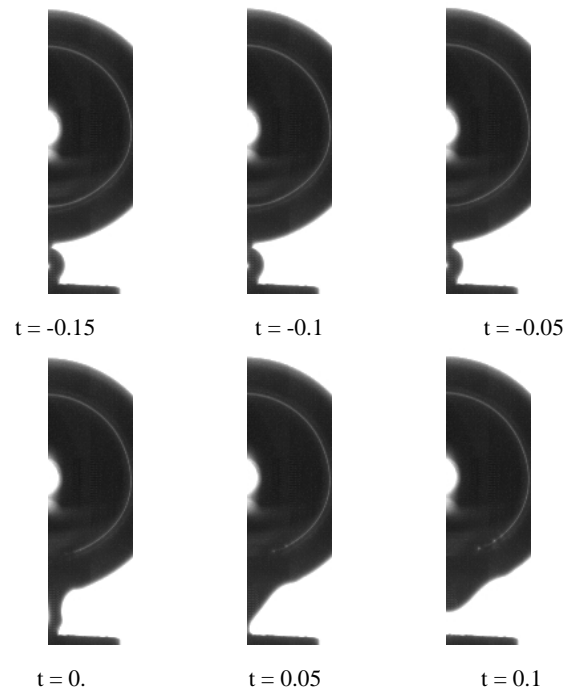


Figure 7: Experimental data for the same times as Figure 6. Unit for the relative time is ms.

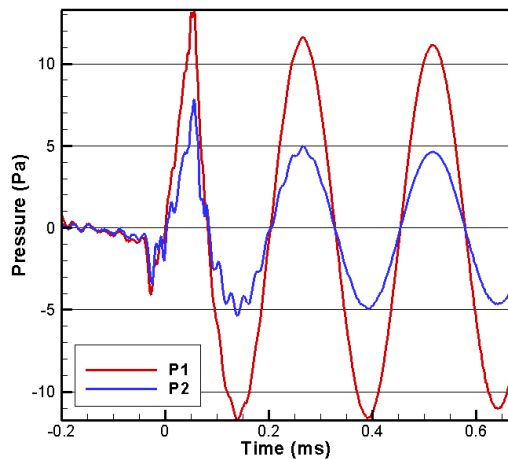


Figure 8: Variation of the pressure.

anism (iii). Laboratory experiments should be conducted in which the size of the secondary bubble could be systematically varied, and in which the added complication of re-attachment could be avoided.

#### Acknowledgments

We are grateful to Sébastien Cazin at IMFT for technical help with the instrumentation and John Davy at CSIRO for valuable discussions.

\*

#### References

- [1] Al-Masry, W. A., Ali, E. M. and Aqeel, Y. M., Determination of bubble characteristics in bubble columns using statistical analysis of acoustic sound measurements, *Chem. Eng. Res. Design*, **83**(A10), 2005, 1196–1207.
- [2] Bhaga, D. and Weber, M. E., In-line interaction of a pair of bubbles in a viscous liquid, *Chem. Eng. Sci.*, **35**, 1980, 2467–2474.
- [3] Boyd, J. W. R. and Varley, J., The uses of passive measurement of acoustic emissions from chemical engineering processes, *Chem. Eng. Sci.*, **56**, 2001, 1749–1767.
- [4] Bui, A. and Manasseh, R., A CFD study of the bubble deformation during detachment, Fifth International Conference on CFD in the Process Industries, Melbourne, Australia, 13–15 December 2006, 2006, Paper 053, Paper 053.
- [5] Chanson, H. and Manasseh, R., Air entrainment processes of a circular plunging jet: void-fraction and acoustic measurements, *J. of Fluids Eng.*, **125**(5), 2003, 910–921.
- [6] Ding, L. and Farmer, D. M., Observations of breaking surface wave statistics, *J. Phys. Oceanogr.*, **24**, 1994, 1368–1387.
- [7] Ellingsen, K. and Risso, F., On the rise of an ellipsoidal bubble in water: oscillatory paths and liquid-induced velocity, *J. Fluid Mech.*, **440**, 2001, 235–268.
- [8] Goharzadeh, A. and Mutabazi, I., Experimental characterization of intermittency regimes in the couette-taylor system, *Eur. Phys. J. B*, **19**, 2001, 157–162.
- [9] Hahn, T. R., Berger, T. K. and Buckingham, M. J., Acoustic resonances in the bubble plume formed by a plunging water jet, *Proc. R. Soc. Lond. A*, **459**, 2003, 1751–1782.
- [10] Hsi, R., Tay, M., Bukur, D., Tatterson, G. B. and Morrison, G., Sound spectra of gas dispersion in an agitated tank, *Chem. Eng. J.*, **31**, 1985, 153–161.
- [11] Hu, Y. Y. and Khoo, B. C., An interface interaction method for compressible multifluids, *J. Comput. Phys.*, **198**, 2004, 35–64.
- [12] Leighton, T. G., *The Acoustic Bubble*, Academic Press, London, 1994.
- [13] Leighton, T. G., Fagan, K. J. and Field, J. E., Acoustic and photographic studies of injected bubbles, *Eur. J. Phys.*, **12**, 1991, 77–85.
- [14] Leighton, T. G. and Walton, A. J., An experimental study of the sound emitted by gas bubbles in a liquid, *Eur. J. Phys.*, **8**, 1987, 98–104.
- [15] Liow, J. L., Splash formation by spherical drops, *J. Fluid Mech.*, **427**, 2001, 73–105.
- [16] Loewen, M. R. and Melville, W. K., Microwave backscatter and acoustic radiation from breaking waves, *J. Fluid Mech.*, **224**, 1991, 601–623.
- [17] Longuet-Higgins, M. S., Monopole emission of sound by asymmetric bubble oscillations. part 1. normal modes, *J. Fluid Mech.*, **201**, 1989, 525–541.
- [18] Longuet-Higgins, M. S., Monopole emission of sound by asymmetric bubble oscillations. part 2. an initial-value problem, *J. Fluid Mech.*, **201**, 1989, 543–565.
- [19] Longuet-Higgins, M. S., An analytic model of sound production by raindrops, *J. Fluid Mech.*, **214**, 1990, 395–410.
- [20] Longuet-Higgins, M. S., Kerman, B. R. and Lunde, K., The release of air bubbles from an underwater nozzle, *J. Fluid Mech.*, **230**, 1991, 365–390.
- [21] Manasseh, R., Bubble-pairing phenomena in sparging from vertical-axis nozzles, 24th Australian & NZ Chemical Engineering Conference, Sydney, 30 Sep - 2 Oct, 1996, volume 5, 27–32, 27–32.
- [22] Manasseh, R., A. Babanin, Forbes, C., Rickards, K., Bobevski, I. and Ooi, A., Passive acoustic determination of wave-breaking events and their severity across the spectrum, *J. Atmos. Ocean Tech.*, **23**(4), 2006, 599–618.
- [23] Manasseh, R., Bui, A., Sanderkot, J. and Ooi, A., Sound emission processes on bubble detachment, 14th Australasian Fluid Mechanics Conference, Adelaide University, Adelaide, Australia, 10-14 December 2001, 2001.
- [24] Manasseh, R., LaFontaine, R. F., Davy, J., Shepherd, I. C. and Zhu, Y., Passive acoustic bubble sizing in sparged systems, *Exp. Fluids*, **30**(6), 2001, 672–682.
- [25] Manasseh, R., Nikolovska, A., Ooi, A. and Yoshida, S., Anisotropy in the sound field generated by a bubble chain, *J. Sound Vibration*, **278** (4-5), 2004, 807–823.
- [26] Manasseh, R., Yoshida, S. and Rudman, M., Bubble formation processes and bubble acoustic signals, Third International Conference on Multiphase Flow, Lyon, France, 8-12 June, 1998.

- [27] Melville, W. K., Loewen, M., Felizardo, F., Jessup, A. and Buckingham, M., Acoustic and microwave signatures of breaking waves., *Nature*, **336**, 1988, 54–56.
- [28] Minnaert, M., On musical air bubbles and the sound of running water, *Phil. Mag.*, **16**, 1933, 235–248.
- [29] Nevers, N. D. and Wu, J.-L., Bubble coalescence in viscous fluids, *Am. Inst. Chem. Eng. J.*, **17**, 1971, 182–186.
- [30] Nikolovska, A., *Passive acoustic transmission and sound channelling along bubbly chains*, Department of Mechanical and Manufacturing Engineering, University of Melbourne, Australia, 2005.
- [31] Oğuz, H. and Prosperetti, A., Numerical calculation of the underwater noise of rain, *J. Fluid Mech.*, **228**, 1993, 417–442.
- [32] Osher, S. and Sethian, J., Fronts propagating with curvature-dependent speed: algorithms based on hamilton-jacobi formulations, *J. Comp. Phys.*, **79**, 1988, 12–49.
- [33] Prosperetti, A. and Oğuz, H., The impact of drops on liquid surfaces and the underwater noise of rain, *Ann. Rev. Fluid Mech.*, **25**, 1993, 577–602.
- [34] Pumphrey, H. C. and Crum, L. A., Free oscillations of near-surface bubbles as a source of the underwater noise of rain, *J. Acous. Soc. Am.*, **87**, 1990, 142–148.
- [35] Pumphrey, H. C. and Elmore, P. A., The entrainment of bubbles by drop impacts, *J. Fluid Mech.*, **220**, 1990, 539–567.
- [36] Rayleigh, On the pressure developed in a liquid during the collapse of a spherical cavity, *Phil. Mag.*, **34**, 1917, 94–98.
- [37] Stewart, C. W., Bubble interaction in low-viscosity liquids, *Int. J. Multiphase Flow*, **21(6)**, 1995, 1037–1046.
- [38] Strasberg, M., The pulsation frequency of nonspherical gas bubbles in liquid, *J. Acoustical Soc. of America*, **25(3)**, 1953, 536–537.
- [39] Strasberg, M., Gas bubbles as sources of sound in liquid, *J. Acoustical Soc. of America*, **28(1)**, 1956, 20–26.
- [40] Yoon, S. and Yabe, T., The unified simulation for incompressible and compressible flow by the predictor-corrector scheme based on the cip method, *Computer Phys. Communications*, **119**, 1999, 149–158.
- [41] Yoshida, S., Manasseh, R. and Kajio, N., The structure of bubble trajectories under continuous sparging conditions, 3rd International Conference on Multiphase Flow, Lyon, France, June 1998, 1998, 426 1–8, 426 1–8.